



Nonlinear refractive index measurement by SPM-induced phase regression

PIOTR KABACIŃSKI,^{1,2,*} TOMASZ M. KARDAŚ,² YURIY STEPANENKO,² AND Czesław RADZEWICZ^{2,3}

¹*Faculty of Physics, Warsaw University of Technology, Koszykowa 75, 00-662 Warsaw, Poland*

²*Institute of Physical Chemistry Polish Academy of Sciences, Kasprzaka 44/52, 01-224 Warsaw, Poland*

³*Institute of Experimental Physics, Faculty of Physics, University of Warsaw, Pasteura 5, 02-093 Warsaw, Poland*

*kabacinski@protonmail.com

Abstract: Herewith, we describe how intensity and phase of the ultrashort pulse retrieved with second-harmonic frequency-resolved optical gating (SHG FROG) can be utilized for measurement of the nonlinear refractive index (n_2). Through comparison with available literature, we show that our method surpasses Z-scan in terms of precision by a factor of two and thus constitutes an interesting alternative. We present results for various materials: fused silica, calcite, YVO_4 , BiBO , CaF_2 , and YAG at 1030 nm. Unlike the Z-scan, the use of this method is not restricted to free-space geometry, but due to its characteristics, it can be used in integrated waveguides or photonic crystal fibers as well.

© 2019 Optical Society of America under the terms of the [OSA Open Access Publishing Agreement](#)

1. Introduction

The optical Kerr effect manifests itself through self-action of high intensity pulses both spatially, through self-focusing, and in spectral domain, through self-phase modulation (SPM). SPM as well as self-focusing enable generation of ultrashort laser pulses. Self-focusing is the basis for widely used Kerr-lens laser modelocking [1, 2] while modelocking of fiber lasers requires assistance of SPM [3] or cross-phase modulation [4]. At the same time the creation of ultrabroad spectra through supercontinuum generation in bulks and liquids is initiated by self-focusing [5, 6] and governed by SPM in fibers [7, 8]. The Optical Kerr Effect also limits the efficiency of optical devices that are based on the second order nonlinear effects, like second harmonic or sum and difference frequency generation [9, 10]. Therefore, precise value, and thus, precise measurement of n_2 is of essence for purposes of designing novel nonlinear optical devices.

Currently Z-scan [11] is the most popular method of n_2 measurement, although, other techniques like: nonlinear interferometry [12–14], degenerate four-wave mixing [15], nearly degenerate three-wave mixing [16, 17], ellipse rotation [18], Moiré deflectometry [19] and beam-distortion measurements [20] are also used. Z-scan involves scanning the sample through the focus of intense, tightly focused laser beam. As the self-focusing effect shifts the effective focal point in space, it lets different amounts of light through the aperture which is shielding the photodiode. Spatial properties of the beam are crucial for proper measurement in this case, since light intensity transmitted through aperture is directly measured. This often requires the characterization of M^2 of the laser beam before Z-scan takes place. The accuracy of this technique is rarely better than 10% with record of 5% for fused silica [21].

An interesting alternative to methods mentioned above can be obtained by employing the pulse electric field reconstruction techniques. The Frequency-Resolved Optical Gating (FROG) setup is nowadays a common equipment in optical laboratories dealing with ultrashort pulses and the software is available online [22, 23]. Using FROG, n_2 has been measured in fused silica and KDP [24], with the authors estimating their result's uncertainty to be 10%. Similar measurements using SPIDER were also conducted in liquid [25] and gas [26] phase, but in both

cases no rigorous n_2 calculation technique was stated. Moreover, in either of those works, no error estimation coming from the method used (FROG or SPIDER) was included in the total uncertainty estimation. Therefore, it couldn't be directly compared to Z-scan, and its limitations were not discussed in detail.

In this work we present an improvement on the idea of Kerr constant measurement through the pulse electric field reconstruction, precisely defining the fitting procedure and including errors coming from FROG retrieval algorithm described in [27] as bootstrap method. Nonlinear refractive index is measured for 6 different samples: fused silica, calcite, YVO₄, CaF₂, YAG and BiBO at 1030 nm. Through the fitting of the SPM-induced phase of the ultrashort pulse – measured with FROG – to the phase expected from SPM self-action – calculated from the temporal intensity envelope of the pulse – the nonlinear index is measured, and different error sources are assessed. We show that this method is a reliable mean of measuring n_2 , with errors on the order of half of those reported in recent Z-scan measurements. Moreover, proposed method can be extended to geometries in which Z-scan cannot operate. Importantly, such geometries include step-index and photonic crystal fibers, as well as integrated waveguides. Possessing this advantage can aid in designing novel optical devices utilizing SPM and self-focusing as a critical part of their working mechanism.

2. Method

The method is based on the observation, that for pulses with moderate spectral widths and thin samples, the dependence of n_2 on frequency, as well as the linear refractive index, can be neglected. Moreover, we assume that no significant dispersion occurs and that there is no change in intensity profile of the pulse. At the same time, the Raman response of the medium can be included into the Kerr effect. In such case, the phase acquired by the pulse depends on the temporal profile of the pulse intensity through:

$$\Delta\phi(t) = n_2 \frac{2\pi d}{\lambda} I(t), \quad (1)$$

where d is the thickness of the sample, λ is the central wavelength of the pulse and $I(t)$ is the light intensity. Equation (1) can be used for calculation of n_2 if both: the change of phase and the intensity of light are known. These two characteristics can be obtained through complete electric field reconstruction of a pair of pulses: the initial pulse $(\phi_i(t), I_i(t))$, and the pulse which has passed through the sample $(\phi_s(t), I_s(t))$. Then:

$$\Delta\phi(t) = \phi_s(t) - \phi_i(t) \quad (2)$$

and any of $I_i(t)$, $I_s(t)$ or their average could in principle be used as the intensity in Eq. (1) as in pure SPM process there is no modification of the temporal intensity profile.

At the same time, the degree to which $I_s(t)$ and $I_i(t)$ are similar can be used as a measure of validity of the assumptions given in first sentences of this section. Steps required to calculate n_2 from pulse measurement are shown in Fig. 1 below.

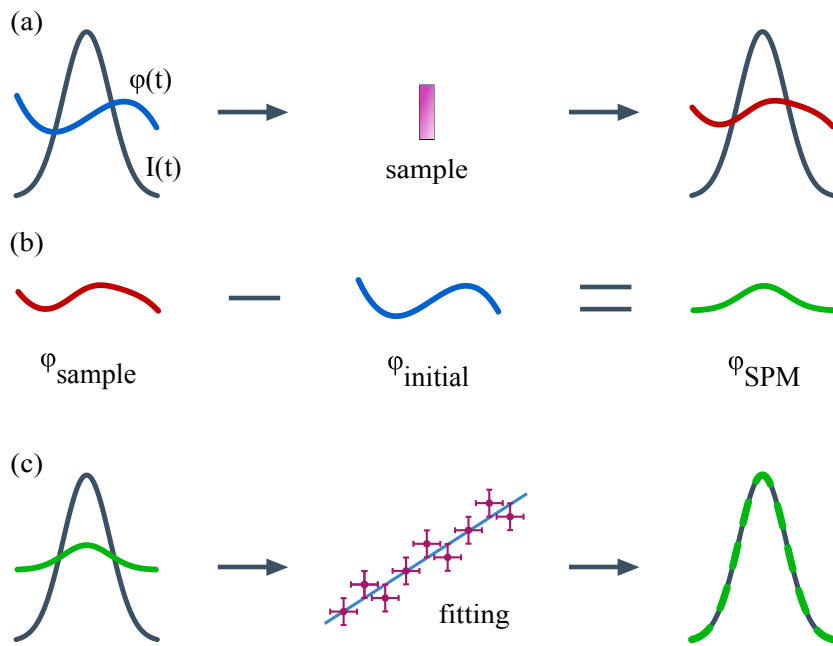


Fig. 1. Schematic description of the method of nonlinear index of refraction measurement. (a) First, the known ultrashort pulse is propagated through the sample to be measured, which modifies its phase via self-phase modulation, whilst having little effect on the intensity envelope. (b) Subtraction of the phase of the initial pulse from the phase measured after propagation through the sample yields SPM-induced phase component. (c) Intensity and the SPM-induced phase are fitted together and according to Eq. (1) the value of n_2 is obtained.

3. Experimental setup

The measurement setup was constructed according to Fig. 2. A Light Conversion PHAROS Ytterbium-based laser system was used as a 1 kHz repetition rate source of 210 fs pulses at a center wavelength of 1030 nm. Half-wave plate and a thin-film polarizer were used as a power control unit. Before interaction with the sample, the beam size was shrank with focusing lens ($f = 250$ mm) and convex mirror ($R = 75$ mm) telescope. This allowed us to obtain weakly focused beam with a Rayleigh range of about 20 cm. Therefore, the sample position didn't need to be critically aligned, and the influence of self-focusing was also mitigated. The beam waist at the focus was measured to be $254 \pm 3 \mu\text{m}$. The pulse from such a beam accumulates nonlinear phase in a thin sample of measured material. After passing through the sample, the pulse is attenuated via first: a reflection from fused silica prism and second: an absorption filter. Next, home-built FROG setup is used for characterization of the pulses with the nonlinear phase imprinted on them. The energy reduction before characterization prevents further accumulation of nonlinear phase in the beamsplitter and sum-frequency crystal within the FROG setup. SHG FROG spectrogram for the pulse is recorded twice, with and without the sample in the setup.

Several samples were measured in this setup: fused silica (3 mm thickness, Eksma Optics), yttrium aluminum garnet (YAG – 2 mm, HG Optronics), calcium fluoride (CaF_2 – 2.63 mm, HG Optronics), calcium carbonate (calcite - 2 mm, both polarization's, Crylight Photonics), yttrium orthovanadate (YVO_4 – 2 mm, both polarization's, Crylight Photonics) and bismuth triborate (BiBO – 2 mm, with electric field along X axis, Foctek).

The samples were not anti-reflection coated, so the Fresnel reflection at the air/sample interface was included in calculations.

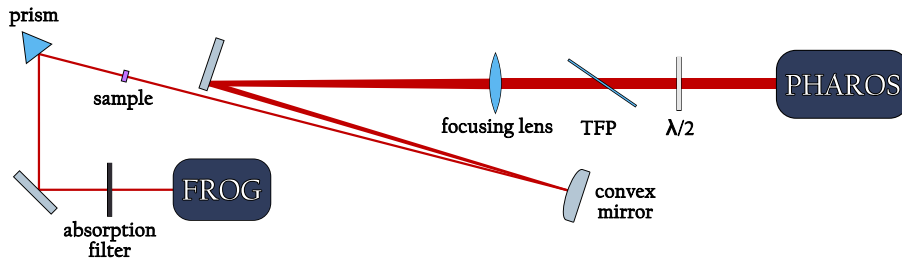


Fig. 2. Measurement setup used in the experiment. Femtosecond pulses are weakly focused onto the sample and after attenuation of the beam are characterized via the FROG apparatus.

Pulse energies ranging from 10 to 180 μJ were used, and the highest available intensity was 420 GW/cm². FROG spectrograms were recorded for different peak powers, to get a statistical distribution of measured values of n_2 , minimize the error, and test the intensity boundaries of the method.

4. Data analysis

Retrieval of the electric field of the pulse from the measured FROG traces was performed with Principal Components Generalized Projections algorithm (PCGPA) [28] implemented in MATLAB. Writing our own program [23] allowed us to incorporate bootstrap error estimation for FROG described in [27].

The basis for bootstrap method is random resampling with replacement of the measured FROG trace, and omission of pixels not drawn in the intensity replacement step within the PCGPA.

Each measured FROG spectrogram was interpolated on the 128x128 grid according to practical measures described in [29]. As the PCGPA algorithm is seeded with random noise it can converge to slightly different results each time, therefore, for the highest possible precision, the algorithm has been evaluated 30 times for the whole FROG trace and the result with lowest error was chosen as the retrieval result (which we denote as the "ordinary" run). Then, for the purpose of error estimation 100 bootstrap runs were done. To ensure high accuracy for all the runs (both "ordinary" and bootstrap) each run consisted of 500 iterations of the algorithm and the lowest FROG error result was chosen each time. Such a procedure carried out for one measured FROG trace took 3 minutes of computation time on a standard personal computer.

The information on the direction of time axis is lost in FROG based on SHG. The otherwise known sign of n_2 , however, determines the curvature of the SPM-induced phase of the pulses, which is directly linked with the direction of the time axis. Therefore, the axis can be reversed for some of the retrieved pulses to keep consistency with the deduced direction.

The temporal position of the retrieved pulse is arbitrary, therefore, in the algorithm the center of mass of the retrieved temporal profile is shifted to $t = 0$. Moreover, for each pulse obtained from bootstrap runs, a shift is performed in relation to the pulse obtained from the "ordinary" run, to maximize overlap between the two pulses. Then, constant value is added to each phase, such that the overlap of the phases is maximized. After the best overlap is ensured, standard deviation in each point of time is calculated for the intensity and the phase, and the error bars equal to this standard deviation are placed on the plot of the retrieved pulse (see for example Fig. 3(a)).

Prepared as such, the pulse measured for specific power and specific sample, and the reference pulse, measured without the sample in the beam path are used as the input for the second stage.

Then, the intensities of the two pulses are compared against each other. Simply plotting both of them helps to estimate if the measurement has been done correctly, as the intensities should be identical within the error range if no significant dispersion, or other intensity shape modifying processes occurred. If it is so, phase contribution caused by SPM can be calculated as a difference between the phase of the pulse going through the sample, and the phase of the pulse measured without the sample in the beam path.

Next, using experimental parameters, intensity in real units is calculated from the normalized intensity retrieved by FROG algorithm (with power corrected for Fresnel reflection on the face of the sample). Assuming that the difference in phase between reference and measured pulses is due to SPM alone, the following Eq. (3) is used for weighted fitting with Levenberg-Marquardt algorithm to find n_2 :

$$\Delta\phi(t) = n_2 \frac{2\pi d}{\lambda} I(t) + at + b, \quad (3)$$

where n_2 , a and b are used as fitting parameters (for detailed description of fitting procedure and error propagation see Appendix A). The linear term can by all means exist in the Taylor expansion of the intensity envelope, and thus, can still cause modification of the phase through SPM. The FROG algorithm is, however, not capable of retrieving the both linear and constant phase components. Therefore, the addition of the $at + b$ term is necessary.

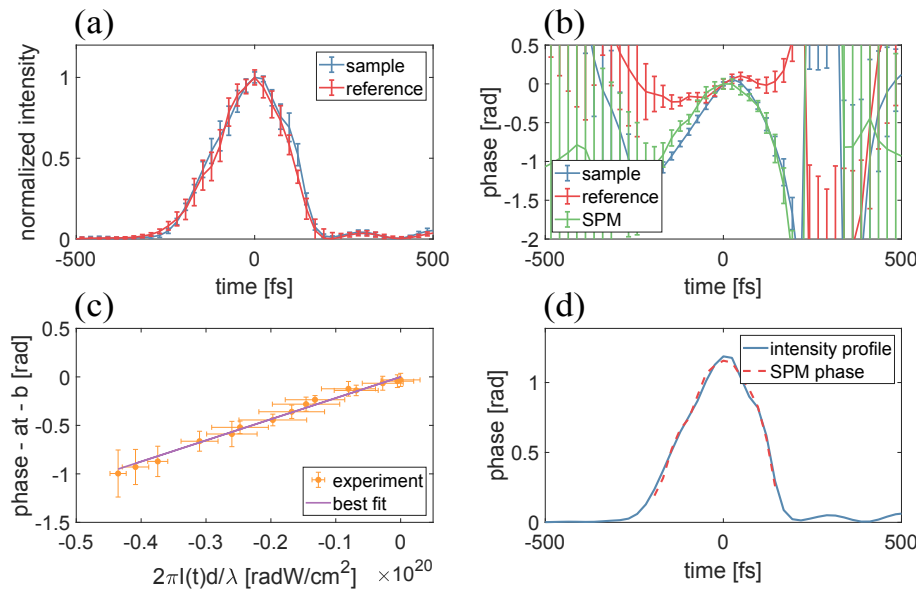


Fig. 3. Procedure of fitting SPM-induced phase to intensity profile for measuring n_2 in fused silica for 160 μ J. (a) Visual comparison of intensity profiles for a pulse propagated through the sample and a reference pulse. (b) Subtraction of the reference phase from the phase measured after propagation through the sample. Their difference is the SPM-induced component of the phase. (c) Phase predicted from intensity profile is fitted to the measured SPM-induced phase. Best fit line is described by Eq. (3). Slope of the purple line presented here is equal to n_2 value for measured material. (d) Intensity profile scaled according to Eq. (3) is compared to the measured SPM-induced phase, showing almost perfect agreement.

The fitting weights are equal to the inverse of the square of the errors in each point of time. Errors of the phase are used directly, and errors of the intensity are projected onto the y-axis using effective variance method [30] (for detailed description see Appendix A). In this particular case where the relation of phase and intensity is linear, the method is exact rather than approximated, as the name would suggest (see Fig. 3(c)). A few iterations of the fitting with weights recalculated within are done to ensure convergence.

In our particular case, a phase discontinuity (π jump) can be observed in the vicinity of the intensity minimum between the main pulse and the intensity lobes that follow it. This is expected as the lobes themselves appear most likely due to the uncompensated third order spectral phase of the input pulses, and in consequence the interference of different spectral components [31]. Moreover, for low intensity, the phase error increases and the phase itself becomes completely unknown in areas where no intensity is present. Therefore, to avoid fitting the phase discontinuity and regions of undefined phase, the fitting range was selected as the area where the intensity values are higher than 15% of its maximum value.

5. Results

The power ranges were selected based on the approximate value of n_2 for each sample. Too low intensity would prevent proper phase difference retrieval, but on the other hand, the high intensity would eventually cause beam distortion due to self-focusing and pulse temporal elongation due to dispersion of the SPM-broadened spectrum.

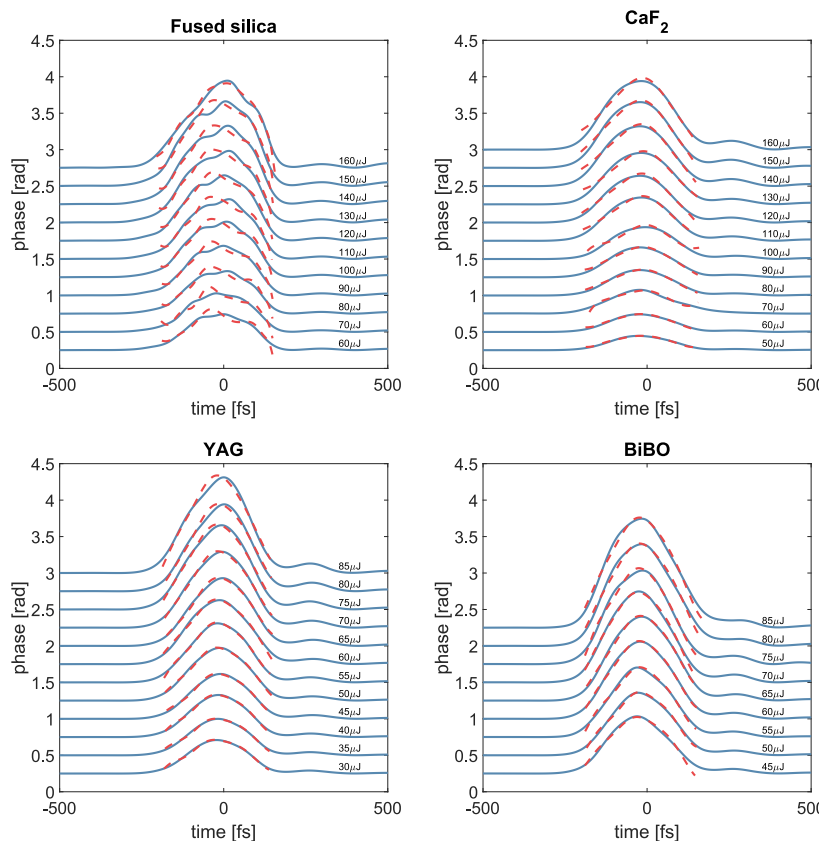


Fig. 4. SPM-induced phases (dashed red) fitted to intensity profiles (blue) for different incident pulse energies for fused silica, CaF₂, YAG and BiBO.

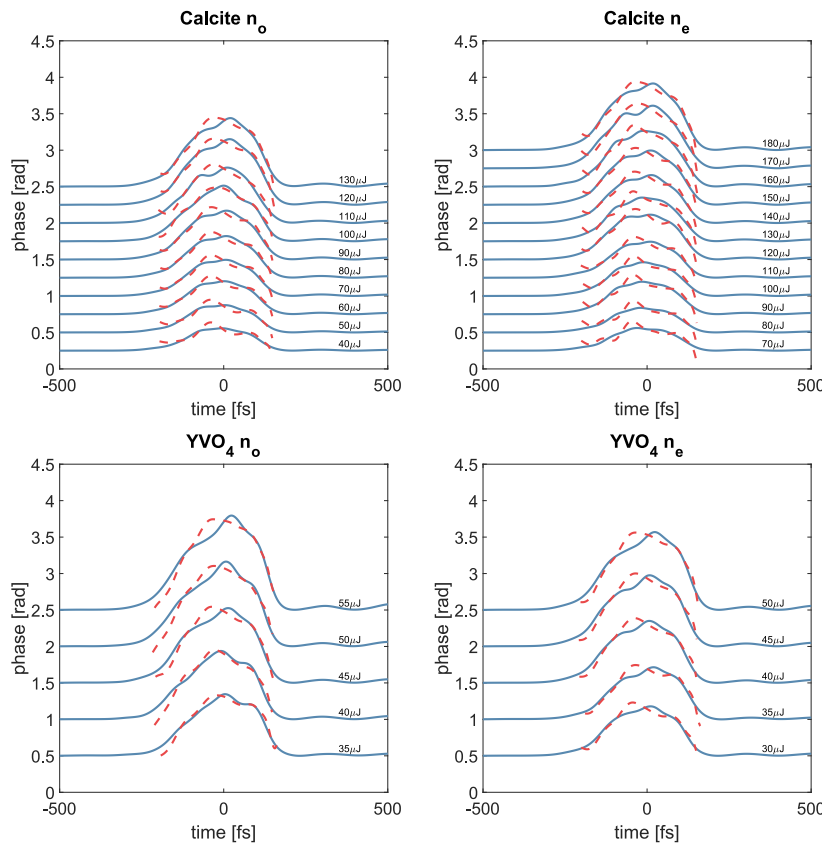


Fig. 5. SPM-induced phases (dashed red) fitted to intensity profiles (blue) for different incident pulse energies for birefringent materials: Calcite and YVO₄.

Measurements were performed for two slightly different adjustments of the phase of the pulse incident on the sample. The phase was varied with the laser built-in compressor. Fused silica, Calcite and YVO₄ were measured for a pulse with a phase slightly oscillating around zero, and CaF₂, BiBO and YAG were measured for a pulse with smooth but less flat phase. Retrieving structured phases oscillating around zero proved difficult for the FROG algorithm in the past [32], and this is also consistent with our observations. Therefore, it is advised to use a starting pulse with non-zero initial phase, so the reference phase is most precisely retrieved by the FROG algorithm.

Measurements in which the phase heavily differed from the intensity profile due to small pulse energy used, and those, where the pulse after propagation through the sample differed much from the reference intensity due to too high pulse energy, were discarded. All of the other measurements are presented in Fig. 4 and Fig. 5 and were used for the final n_2 value calculation. As can be seen, the shape of the SPM-induced phase resembles the intensity profile shape well throughout different samples and pulse energies.

Final n_2 value for each sample was calculated as the weighted average of values measured for different energies (see Fig. 6). Our results together with their error (see Appendix A) have been compared with values found in the literature, measured with Z-scan, as in Table 1.

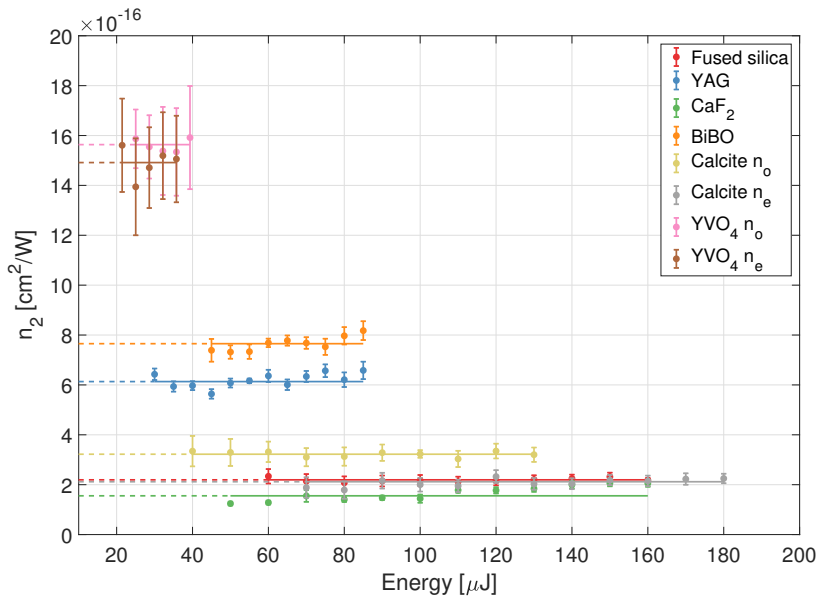


Fig. 6. All measured n_2 values for varying pulse energy for different samples. Straight lines are weighted averages of values for given sample.

Table 1. Nonlinear Refractive Index Measured in This Work at 1030 nm Compared with Values Known from Literature^a

Material	This work	Literature
Fused silica	2.19 ± 0.05	2.23 ± 0.12 at 1030 nm [21]
		2.74 ± 0.17 at 1053 nm [33]
		2.46 at 1064 nm [17]
CaF_2	1.71 ± 0.09	1.9 ± 0.26 at 1064 nm [34]
		1.26 at 1064 nm [17]
YAG	6.13 ± 0.07	6.25 at 1064 nm [17]
		7.23 ± 1.4 at 1064 nm [35]
BiBO $E X$	7.65 ± 0.09	$7.39, 8.00$ at 1064 nm [36]
Calcite n_o	3.22 ± 0.09	2.83 at 1064 nm [17]
Calcite n_e	2.12 ± 0.07	2.35 at 1064 nm [17]
$YVO_4 n_o$	15.6 ± 0.7	19 at 1080 nm in Yb:YVO ₄ [37]
$YVO_4 n_e$	14.9 ± 0.8	15 at 1080 nm in Yb:YVO ₄ [37]

^aAll values are in units of $10^{-16} \frac{cm^2}{W}$.

Measured values present good agreement with the literature. Lowest relative error is 1.1% for YAG and the highest is 5.4% for YVO₄. Note, however, that for highly nonlinear YVO₄ the number of measurements was limited. For fused silica our method has twice as low error as previously reported in z-scan measurements [21]. For the case of CaF₂ we observe a slight growth of the n₂ value with pulse energy. It is unlikely that the higher order nonlinearity of CaF₂ is responsible for this behaviour. On the other hand, limited purity of the sample or thermally induced refractive index could be an explanation here.

6. Conclusion

In this work, measurement of nonlinear refractive index of several optical materials via FROG pulse reconstruction and fitting the intensity to the SPM-induced phase was critically investigated. Measurements in wide power range were conducted to test the limits of the method. Including the bootstrap method for error estimation of FROG-retrieved pulses allowed to account for all error sources and to compare precision with other studies.

Our results show that the described method is well defined and precise, and as such, it is a direct competitor to Z-scan. As long as there is enough power in the pulse for the FROG method to resolve the phase, and the sample is thin enough to avoid dispersion reshaping the pulse, the method works very well in wide range of experimental parameters. Considering that in this scheme the nonlinear phase is characterized directly, it is not restricted to free-space geometries and unlike Z-scan, can be used for characterization of nonlinearity in integrated waveguides or photonic crystal fibers.

Appendix A: Detailed scheme of calculation of n₂ and its uncertainty

The value and uncertainty of the nonlinear refractive index is calculated according to the following procedure:

1. Sample and reference intensity profiles ($I_s(t), I_r(t)$), phases ($\phi_s(t), \phi_r(t)$) and their uncertainties ($I_s^{err}(t), I_r^{err}(t), \phi_s^{err}(t), \phi_r^{err}(t)$) are calculated from FROG signals with the bootstrap method (see Fig. 3(a) for sample results).
2. The SPM induced phase difference ($\phi_{SPM}(t) = \phi_s(t) - \phi_r(t)$) and its uncertainty ($\phi_{SPM}^{err}(t) = \sqrt{(\phi_s^{err}(t))^2 + (\phi_r^{err}(t))^2}$) is then calculated (see Fig. 3(b) for sample results).
3. The theoretical phase normalised to unitary value of n₂ is calculated from sample intensity profile:

$$\phi_t = \frac{2\pi d}{\lambda} I_s = \frac{2\pi d}{\lambda} \frac{E}{\pi w_0^2} \frac{I_s}{\int I_s dt}$$

with E being the measured energy of the pulse, and the uncertainty follows from propagation theory [38]:

$$\phi_t^{err} = \sqrt{\sum_p \left(\frac{d\phi_t}{dp} p^{err} \right)^2} = \phi_t \sqrt{\left(\frac{I_s^{err}}{I_s} \right)^2 + \left(\frac{\lambda^{err}}{\lambda} \right)^2 + \left(\frac{d^{err}}{d} \right)^2 + \left(\frac{E^{err}}{E} \right)^2 + 4 \left(\frac{w_0^{err}}{w_0} \right)^2}$$

with p enumerating parameters of ϕ_t .

4. Levenberg-Marquardt least squares algorithm is used for fitting of an expression: $n_2 \phi_t(t) + at + b$ to: $\phi_{SPM}(t)$. The necessity of using additional parameters a and b is described in section 4. of the manuscript. Figure 3(c) presents example fit. The fitting procedure is performed five times with different fit weights ($W_j, j \in [1, 5]$). The first fit uses:

$$W_1 = \frac{1}{(\phi_{SPM}^{err})^2}$$

and for iterations that follow the effective variance approximation [30] is used:

$$W_j = \frac{1}{(\phi_{SPM}^{err})^2 + (n_{2,j-1}\phi_t^{err})^2}$$

The $n_2 = n_{2,5}$ and its uncertainty n_2^{err} for a particular pulse energy is obtained from the last fit ($j = 5$).

5. The final result is obtained with weighted averaging [38] of results obtained for k different pulse energies (enumerated by $i \in [1, k]$):

$$\bar{n}_2 = \frac{\sum_i^k n_{2,i}/n_{2,i}^{err}}{\sum_i^k 1/n_{2,i}^{err}}, \quad \bar{n}_2^{err} = \sqrt{\max(\sigma_{int}^2, \sigma_{ext}^2)}$$

where

$$\sigma_{int}^2 = \frac{1}{\sum_i^k 1/n_{2,i}^{err}} \quad \text{and} \quad \sigma_{ext}^2 = \frac{\sigma_{int}^2}{k-1} \sum_i^k \left(\frac{n_{2,i} - \bar{n}_2}{n_{2,i}^{err}} \right)^2$$

Funding

Office of Naval Research Global (N62909-14-1-N229); National Science Center, Poland (2017/25/B/ST7/01145).

Acknowledgments

We kindly acknowledge Prof. Wojciech Gadomski and Dr. Kamil Polok for lending us the CaF₂ and YAG samples.

References

1. D. E. Spence, P. N. Kean, and W. Sibbett, "60-fsec pulse generation from a self-mode-locked Ti:sapphire laser," *Opt. Lett.* **16**, 42 (1991).
2. V. P. Kalosha, M. Müller, J. Herrmann, and S. Gatz, "Spatiotemporal model of femtosecond pulse generation in Kerr-lens mode-locked solid-state lasers," *JOSA B* **15**, 535–550 (1998).
3. J. Szczepanek, T. M. Kardaś, M. Michalska, C. Radzewicz, and Y. Stepanenko, "Simple all-PM-fiber laser mode-locked with a nonlinear loop mirror," *Opt. Lett.* **40**, 3500 (2015).
4. J. Szczepanek, T. M. Kardaś, C. Radzewicz, and Y. Stepanenko, "Nonlinear polarization evolution of ultrashort pulses in polarization maintaining fibers," *Opt. Express* **26**, 13590 (2018).
5. R. R. Alfano and S. L. Shapiro, "Direct distortion of electronic clouds of rare-gas atoms in intense electric fields," *Phys. Rev. Lett.* **24**, 1217 (1970).
6. R. R. Alfano and S. L. Shapiro, "Observation of self-phase modulation and small-scale filaments in crystals and glasses," *Phys. Rev. Lett.* **24**, 592 (1970).
7. J. M. Dudley, G. Genty, and S. Coen, "Supercontinuum generation in photonic crystal fiber," *Rev. Mod. Phys.* **78**, 1135–1184 (2006).
8. P. S. J. Russell, P. Hölzer, W. Chang, A. Abdolvand, and J. C. Travers, "Hollow-core photonic crystal fibres for gas-based nonlinear optics," *Nat. Photonics* **8**, 278–286 (2014).
9. R. W. Boyd, *Nonlinear Optics* (Elsevier, 2003).
10. R. L. Sutherland, D. G. McLean, and S. Kirkpatrick, *Handbook of Nonlinear Optics* (Marcel Dekker, 2003), 2nd ed.
11. M. Sheik-Bahae, A. A. Said, and E. W. V. Stryland, "High-sensitivity, single-beam n₂ measurements," *Opt. Lett.* **14**, 955–957 (1989).
12. M. J. Weber, D. Milam, and W. L. Smith, "Nonlinear refractive index of glasses and crystals," *Opt. Eng.* **17**, 463–469 (1978).
13. M. J. Moran, C. Y. She, and R. L. Carman, "Interferometric measurements of nonlinear refractive-index coefficient relative to CS₂ in laser-system-related materials," *IEEE J. Quantum Electron.* **11**, 259–263 (1975).
14. D. Cotter, C. N. Ironside, B. J. Ainslie, and H. P. Girdlestone, "Picosecond pump-probe interferometric measurement of optical nonlinearity in semiconductor-doped fibers," *Opt. Lett.* **14**, 317–319 (1989).
15. S. R. Friberg and P. W. Smith, "Nonlinear optical glasses for ultrafast optical switches," *IEEE J. Quantum Electron.* **23**, 2089–2094 (1987).

16. R. Adair, L. L. Chase, and S. A. Payne, "Nonlinear refractive-index measurements of glasses using three-wave frequency mixing," *J. Opt. Soc. Am. B* **4**, 875–881 (1987).
17. R. Adair, L. L. Chase, and S. A. Payne, "Nonlinear refractive index of optical crystals," *Phys. Rev. B* **39**, 3337 (1988).
18. A. Owyong, "Ellipse rotation studies in laser host materials," *IEEE J. Quantum Electron.* **9**, 1064–1069 (1973).
19. S. Rasouli, H. Ghasemi, M. T. Tavassoly, and H. R. Khalesifard, "Application of "parallel" moiré deflectometry and the single beam z-scan technique in the measurement of the nonlinear refractive index," *Appl. Opt.* **50**, 2356–2360 (2011).
20. W. E. Williams, M. J. Soileau, and W. V. Stryland, "Optical switching and n_2 measurements in CS_2 ," *Opt. Commun.* **50**, 256–260 (1984).
21. S. R. Flom, G. Beadie, S. S. Bayya, B. Shaw, and J. M. Auxier, "Ultrafast z-scan measurements of nonlinear optical constants of window materials at 772, 1030, and 1550 nm," *Appl. Opt.* **54**, F123–F128 (2015).
22. K. W. DeLong, "Femtosoftware frog," <https://github.com/kenwdelong/frog> (2014).
23. P. Kabaciński and T. M. Kardaś, "Nonlinear index of refraction measurement by spm-induced phase regression software," <http://doi.org/10.6084/m9.figshare.6894392> (2018).
24. A. J. Taylor, G. Rodriguez, and T. S. Clement, "Determination of n_2 by direct measurement of the optical phase," *Opt. Lett.* **21**, 1812–1814 (1996).
25. S. Couris, M. Renard, O. Faucher, B. Lavorel, R. Chaux, E. Koudoumas, and X. Michaut, "An experimental investigation of the nonlinear refractive index (n_2) of carbon disulfide and toluene by spectral shearing interferometry and z-scan techniques," *Chem. Phys. Lett.* **369**, 318–324 (2003).
26. S. Xu, B. Lavorel, O. Faucher, and R. Chaux, "Characterization of self-phase modulated ultrashort optical pulses by spectral phase interferometry," *J. Opt. Soc. Am. B* **19**, 165–168 (2002).
27. Z. Wang, E. Zeek, R. Trebino, and P. Kvan, "Determining error bars in measurements of ultrashort laser pulses," *J. Opt. Soc. Am. B* **20**, 2400–2405 (2003).
28. D. J. Kane, "Principal components generalized projections: a review," *J. Opt. Soc. Am. B* **25**, A120–A132 (2008).
29. K. W. DeLong, D. N. Fittinghoff, and R. Trebino, "Practical issues in ultrashort-laser-pulse measurement using frequency-resolved optical gating," *IEEE J. Quantum Electron.* **32**, 1253–1264 (1996).
30. D. R. Barker and L. M. Diana, "Simple method for fitting data when both variables have uncertainties," *Am. J. Phys.* **42**, 224–227 (1974).
31. G. Agrawal, *Nonlinear fiber optics* (Academic, 2001).
32. K. W. DeLong, R. Trebino, J. Hunter, and W. E. White, "Frequency-resolved optical gating with the use of second-harmonic generation," *J. Opt. Soc. Am. B* **11**, 2206–2215 (1994).
33. D. Milam, "Review and assessment of measured values of the nonlinear refractive-index coefficient of fused silica," *Appl. Opt.* **37**, 546–550 (1998).
34. D. Milam, M. J. Weber, and A. J. Glass, "Nonlinear refractive index of fluoride crystals," *Appl. Phys. Lett.* **31**, 822–825 (1978).
35. E. S. Bliss, D. R. Speck, and W. W. Simmons, "Direct interferometric measurements of the nonlinear refractive index coefficient n_2 in laser materials," *Appl. Phys. Lett.* **25**, 728–730 (1974).
36. S. Miller, F. Rotermund, G. Xu, F. Noack, V. Panyutin, and V. Petrov, "Polarization-dependent nonlinear refractive index of BiB_3O_6 ," *Opt. Mater.* **30**, 1469–1472 (2008).
37. A. G. Selivanov, I. A. Denisov, N. V. Kuleshov, and K. V. Yumashev, "Nonlinear refractive properties of Yb^{3+} -doped $\text{KY(WO}_4)_2$," *Appl. Phys. B* **83**, 61–65 (2006).
38. A. A. Clifford, *Multivariate Error Analysis: A Handbook of Error Propagation and Calculation in Many-Parameter Systems* (John Wiley and Sons, 1973).